Anniversary Paper: Image processing and manipulation through the pages of *Medical Physics*

Samuel G. Armato III[a)]
Department of Radiology, The University of Chicago, 5841 South Maryland Avenue, Chicago, Illinois 60637

Bram van Ginneken
Image Sciences Institute, University Medical Center Utrecht, Heidelberglaan 100, Room Q0S.459, 3584 CX Utrecht, The Netherlands

(Received 17 June 2008; revised 11 August 2008; accepted for publication 11 August 2008; published 16 September 2008)

The language of radiology has gradually evolved from "the film" (the foundation of radiology since Wilhelm Roentgen's 1895 discovery of x-rays) to "the image," an electronic manifestation of a radiologic examination that exists within the bits and bytes of a computer. Rather than simply storing and displaying radiologic images in a static manner, the computational power of the computer may be used to enhance a radiologist's ability to visually extract information from the image through image processing and image manipulation algorithms. Image processing tools provide a broad spectrum of opportunities for image enhancement. Gray-level manipulations such as histogram equalization, spatial alterations such as geometric distortion correction, preprocessing operations such as edge enhancement, and enhanced radiography techniques such as temporal subtraction provide powerful methods to improve the diagnostic quality of an image or to enhance structures of interest within an image. Furthermore, these image processing algorithms provide the building blocks of more advanced computer vision methods. The prominent role of medical physicists and the AAPM in the advancement of medical image processing methods, and in the establishment of the "image" as the fundamental entity in radiology and radiation oncology, has been captured in 35 volumes of *Medical Physics*. © *2008 American Association of Physicists in Medicine*.
[DOI: 10.1118/1.2977537]

Key words: image processing, segmentation, enhanced visualization, image restoration, image display, informatics, noise reduction, image preprocessing

I. FROM ANALOG FILM TO DIGITAL IMAGES

The radiographic film is an analog device that captures, during exposure, the spatial distribution of light photons that emanate from the phosphor screen in response to the spatial distribution of x-ray photons transmitted through the patient. In its dual role, the radiographic film then serves as an analog device that displays the recorded information as a spatial distribution of transmitted light photons from a source of backlight. As an analog display device, the film must be interpreted by the radiologist purely in a subjective, qualitative manner. Although many aspects of the screen-film-based imaging chain are tuned to accentuate the visual appearance of structures of interest within the anatomic region under evaluation (including beam energy, screen properties, and developer conditions), the developed film remains a static entity that may not be modified to mitigate perceptual limitations of the human eye-brain system. The image captured and displayed on film is very much in accordance with the saying, "What you see is what you get," although magnifying loops and hot-light techniques may be used, along with considerations of lightboard luminance[1] and ambient lighting conditions,[2] to facilitate human perception of the film image.

Analog image enhancement techniques have been reported to enhance film images based predominantly on optical processing approaches.[3–6] Renner and Luke[3] investigated two incoherent-light-based image processing techniques to improve the perception of conventional tomographic images. The first technique was an all-purpose approach based on the Herschel effect, and the second technique simulated a high-pass spatial filter through a film-copying technique. Liu *et al.*[5] used three optical processing architectures that convert the film image into a distribution of coherent light and perform mathematical operations on this coherent light distribution (Fig. 1). Optical frequency filters were implemented to enhance features in mammograms. Panchangam *et al.*[6] used a self-adaptive optical Fourier processing system to selectively display microcalcification clusters or surrounding parenchymal tissue in mammograms. The selection of structures for enhancement was achieved interactively by rotating the analyzer in the optical system.

Despite the qualitative, analog nature of film, quantitative information may be extracted from regions of the film using a microdensitometer,[7] which converts the fraction of light transmitted through the film at different spatial locations into numeric optical density values. A more systematic approach to the quantification of film is through the use of film digitizers, which have been characterized, evaluated, and compared in multiple *Medical Physics* articles (Fig. 2).[8–13] Yin *et al.*[8] combined a curve-fitting technique with an angulated slit image to measure the presampling modulation transfer function (MTF) of two laser scanners and an optical drum scan-

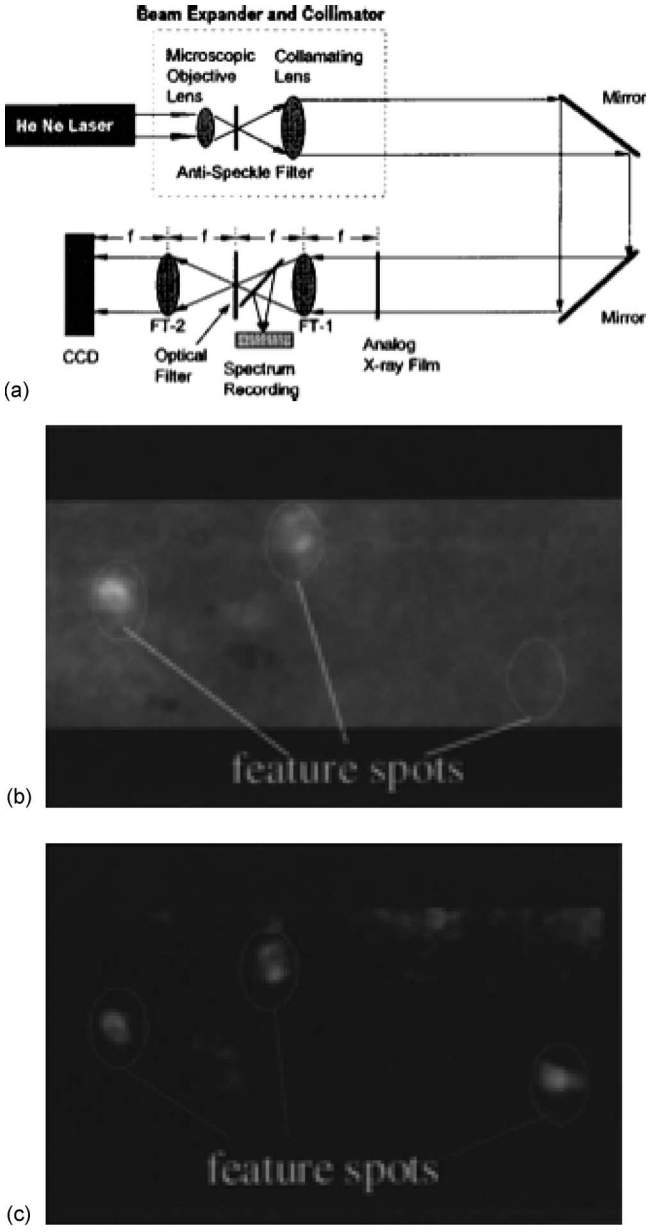

FIG. 1. (a) An (analog) optical processing architecture for analog radiographs. A region of a mammogram (b) prior to and (c) after optical processing. (Reprinted with permission from Ref. 5.)

ner. Meeder *et al.*[10] reported several tests designed to evaluate image transfer characteristics of digitizers, including geometric accuracy, characteristic curve linearity, temporal and spatial response to abrupt optical density changes, and noise contributions. Dempsey *et al.*[12] developed techniques to eliminate interference pattern fluctuation artifacts and light-spread artifacts introduced by film digitizers. The first type of artifact was eliminated through the use of a masked diffusing ground-glass scanning bed, and the second type of artifact was eliminated through application of Fourier-transform-based deconvolution of transmission profiles with measured digitizer line-spread functions.

Hangiandreou *et al.*[11] compared the performance of charged-coupled device (CCD) digitizers and laser digitizers.

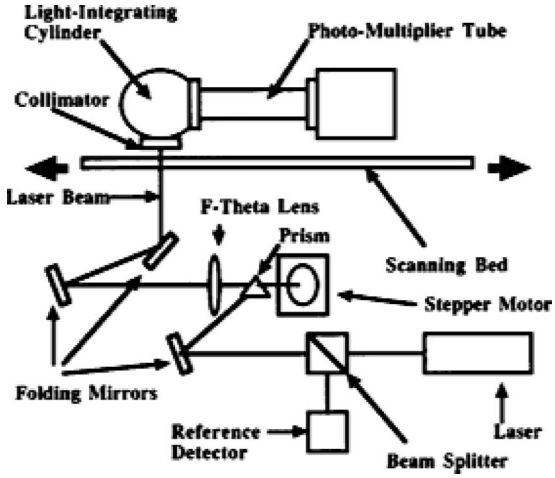

FIG. 2. Schematic diagram of a laser-scanning film digitizer. (Reprinted with permission from Ref. 12.)

A function derived from the Rose model was used to evaluate signal, noise, and useful optical density range, and the investigators found that this function could provide a useful evaluation tool for acceptance testing and quality control. Gonzalez *et al.*[13] continued investigations of CCD digitizers by comparing noise reduction through an increase in signal resolution versus application of a low-pass filter. Other groups have evaluated digitizers for film dosimetry applications.[14–16]

The output of the film digitizer is a digital image: a computer file that contains, at discrete addresses that may be mapped to specific spatial locations of the film, bounded integer values representing the average optical density over a small region of the film at each location. Although the film digitizer is becoming an anachronism, the digital image reigns supreme in radiology, with nearly every diagnostic imaging modality now routinely generating digital image files (mammography is the last modality where screen film is still considered superior by some radiologists). Gone (or at least quickly disappearing) are the days of lost films, bulky patient film folders, space-consuming film libraries, and the need to hang prior films.

II. IMAGE INFORMATICS

These aspects of the film-based radiology department have been replaced by an electronic infrastructure for the storage and retrieval of image data generally known as imaging informatics, the foundation of which is the picture archiving and communication system (PACS). Efforts are underway to integrate imaging informatics with the more global hospital information system[17] to achieve an enterprise-wide approach to image, clinical, and patient demographic information. The role of the medical physicist in the development, implementation, and support of PACS and hospital information systems has been the subject of several Point/Counterpoint articles in *Medical Physics*.[18–20] The various roles of medical physicists and the AAPM in the

evolution of informatics has been nicely reviewed in the Anniversary Paper by Kagadis *et al.*[21]

The ability to integrate, as seamlessly as possible, the PACS environment with medical image acquisition devices and image display (or other output) devices has proven to be a monumental effort of digital image formats, standards, and communications. Of historical note, in 1982, several years before the American College of Radiology and the National Electrical Manufacturers Association released the standard that would later evolve into what has become known as DICOM (Digital Imaging and Communications in Medicine), the AAPM issued Report No. 10 ("A Standard Format for Digital Image Exchange").[22] This report stemmed from a task force formed by the AAPM Science Council to "consider the problem of transferring digital image data between devices." The task force concluded that "it is impractical, at the present time, to adopt a standard internal representation for digital image data acquired and processed by commercially available equipment" due to "incompatibility between the hardware and software used by different manufacturers, and nonuniformity of the formats used for recording the image data on magnetic media." The report, however, provided a magnetic tape format solely for the exchange of digital images. Then, as now (with the DICOM standard), associated descriptive information ("metadata") stored along with the image data was essential to properly understand and manipulate the image structure.

In addition to the metadata stored in the image headers or archive directory structure, methods to interrogate image data could prove useful to a more robust PACS implementation. To facilitate the retrieval of images (specifically radiographic chest images) from a PACS environment, Morishita *et al.*[23] developed an automated patient recognition method based on an image-matching technique that computes the correlation between two images (e.g., a current and previous image) presumed to belong to the same patient. Two posteroanterior (PA) radiographic chest images acquired from the same patient at different times generally yielded a larger correlation value than PA chest images from two different patients. The method was able to correctly identify mismatched previous and current radiographic chest images in over half of the cases in the investigators' database. A method to verify the accuracy of images retrieved from a PACS was developed by Arimura *et al.*[24] Their method applied a template-matching technique to the task of differentiating PA and lateral radiographic chest images. The "average" PA chest image and the "average" lateral chest image for small, medium, and large patients in a training database were created as the template images against which a novel image was compared (Fig. 3). The view for 1000 test images (500 PA and 500 lateral) was correctly identified.

One burden of digital images is the physical file sizes that can be attained. Large file sizes can greatly magnify storage media requirements and severely hinder file transfer. Image compression techniques may be used to overcome these issues, and a number of compression strategies have been reported in *Medical Physics*.[25–34] Lossless compression of an image manipulates the sequences of bits in the image file so that the decompressed file is exactly the same as the original file.[26] Since practically useful compression ratios generally are not possible with lossless compression techniques, compression strategies for images are "lossy." Lo *et al.*[27] developed a decomposition-based compression method that uses image splitting and gray-level remapping. Yin *et al.*[30] developed a compression method using both wavelet-transform and field-masking techniques. Phelan *et al.*[32] developed a wavelet-based compression method that uses the morphology of wavelet transform coefficients in the wavelet domain to isolate and retain significant coefficients (those that correspond to key image features) and further compress remaining coefficients.

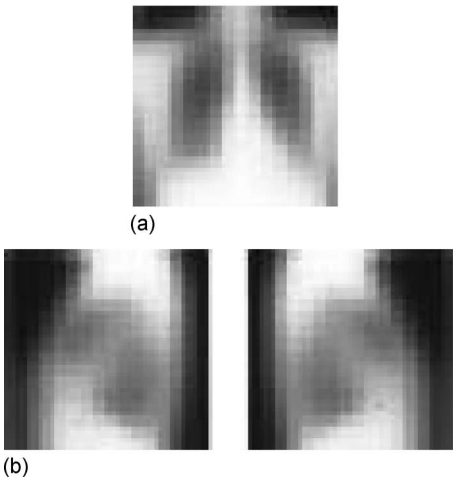

FIG. 3. Examples of (a) a PA template image and (b) lateral template images used in an automated system to differentiate PA and lateral radiographic chest images retrieved from a PACS. (Reprinted with permission from Ref. 24.)

Lossy compression, to be effective, requires a balance between high compression ratios and diagnostic fidelity of the decompressed image. Höhne *et al.*[25] applied Fourier-transform-based compression to digital angiography sequences of the heart and brain and obtained compression ratios between 5:1 and 10:1 without loss of diagnostic information. Cook *et al.*[28] and Cox *et al.*[29] both investigated the detectability of low-contrast objects in images compressed through full-frame discrete cosine transform techniques with varying levels of compression. The contrast-detail phantom experiments of Cook *et al.* identified a statistically significant degradation in detectability for an average compression ratio of 125:1 but not for an average compression ratio of 11:1. Cox *et al.* introduced simulated noncalcified pulmonary nodules into clinical radiographic chest images and, in a series of two-alternative forced choice observer experiments, observed a measurable decrease in performance across compression ratios of 7:1, 16:1, 44:1, and 127:1. Zhao *et al.*[31] used the nonprewhitening matched filter to quantify the effect of wavelet-based compression on lesion detectability through a simulation study. The size, amplitude, and associated noise of simulated signals were varied, along with the compression ratio, to identify combinations of parameters that generated equivalent detectability. Using images from

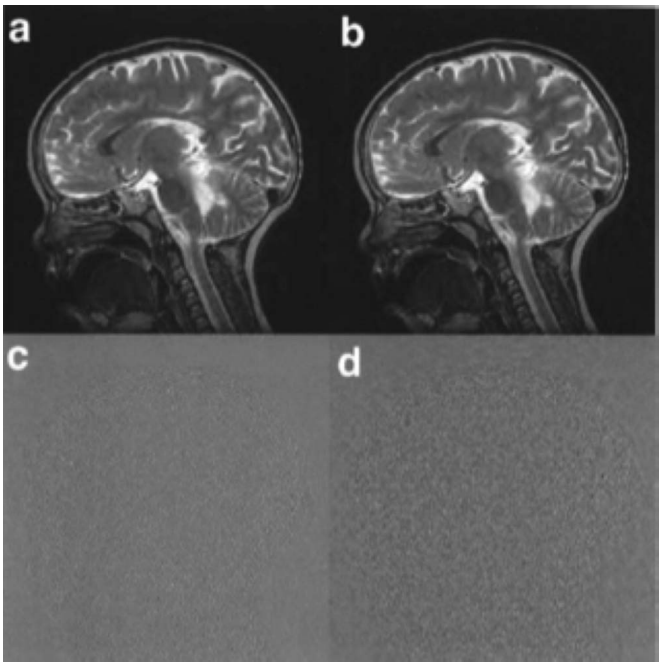

FIG. 4. Magnetic resonance (MR) images after compression and uncompression with the (a) JPEG (discrete cosine transform) and (b) wavelet compression algorithms. The corresponding error images are shown also for the (c) JPEG and (d) wavelet algorithms. (Reprinted with permission from Ref. 33.)

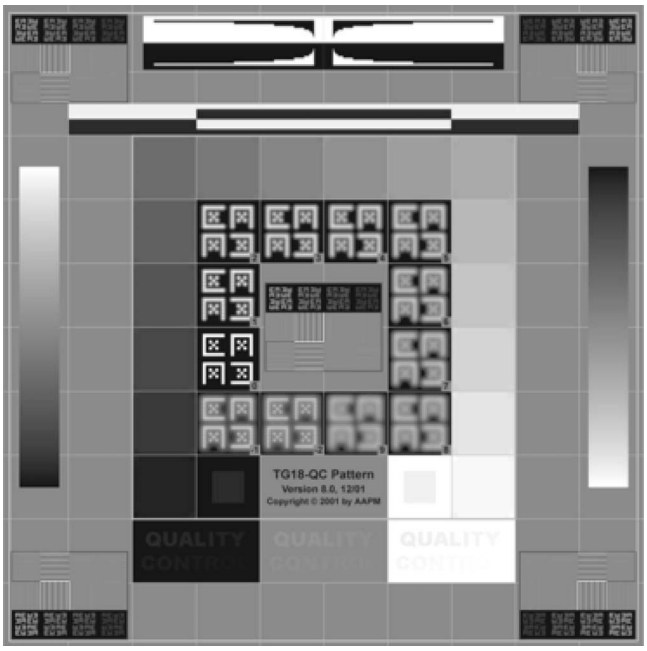

FIG. 5. The TG18-QC test pattern. (Reprinted with permission from Ref. 46.)

six different diagnostic imaging modalities, Thompson *et al.*[33] compared a wavelet-based compression algorithm against a discrete cosine transform compression method. For compression ratios up to 40:1, the wavelet algorithm demonstrated generally lower average error-metric values and higher peak signal-to-noise ratios (Fig. 4). Fidler *et al.*[34] evaluated the influence of image information on compression and image degradation using the JPEG standard. Their qualitative and quantitative findings indicated that image degradation is strongly dependent on image information (as computed from image entropy).

III. IMAGES ON DISPLAY

Digital images have no inherent associated visual representation. The electronic display device ("soft-copy display") fulfills the role of image presentation for the visual consumption of a radiologist. Medical physicists have been intimately involved in the physical characterization and performance assessment of such displays, which require a unique blend of physics and perception.[35–52] These investigations include cathode-ray tube (CRT) displays and liquid crystal displays (LCDs) and monochrome and color display devices. According to AAPM professional guidelines from 1994, "the performance assessment of electronic display devices in healthcare institutions falls within the professional responsibilities of medical physicists."[53] AAPM On-Line Report No. 03 ("Assessment of Display Performance for Medical Imaging Systems") noted that "considering the fundamental importance of display image quality to the overall effectiveness of a diagnostic imaging practice, it is vitally important to assure that electronic display devices do not compromise image quality."[47] This statement was echoed in the Executive Summary of the AAPM TG18 report published in *Medical Physics*.[46] Although early work on the performance assessment of monitors made use of the Society of Motion Picture and Television Engineers test pattern,[38] the AAPM TG18 test patterns (Fig. 5) were quickly adopted by the medical physics community.

Jung *et al.*[45] evaluated the performance of 32 LCDs based on the AAPM TG18 document and test patterns. Their evaluation included the angular dependencies of luminance and contrast, an effect further explored by several other groups.[42,43,48] These studies demonstrated the successful clinical implementation of the AAPM TG18 guidelines for medical display performance assessment and the impact of angular response on image contrast. In an effort to advance these guidelines, Jacobs *et al.*[50] proposed a variable test pattern for the quality assurance assessment of displays. Unlike the test pattern developed by AAPM Task Group 18, the variable pattern included randomly generated elements intended to reduce bias due to observer memory effects.

Observer-based contrast-detail studies have been conducted to quantify the contribution of display-related effects to the detection of simulated lesions in images.[36,37,40,41] Direct comparisons among LCDs and CRT displays have been performed.[49,52] Others have investigated noise in LCDs[44] and the temporal response of LCDs,[51] an important characteristic for proper interpretation of real-time image sequences acquired, for example, during fluoroscopy.

IV. IMAGE RESTORATION

The ability to electronically manipulate images is a powerful benefit to digital image files. Image manipulation tech-

niques have been performed to overcome the limitations of displays or to correct artifacts due to the image acquisition process.[54–58,39,59–66] Moseley and Munro,[39] for example, developed a method to display portal images that permits the user to optimize display contrast without saturating parts of the image. The difference between the average signal in small regions and the global average was subtracted from the original image to reduce changes in average signal that occur over large spatial dimensions without obscuring changes in signal that occur over small spatial dimensions. A method to remove veiling glare from fluoroscopic images was developed by Seibert *et al.*[54] based on deconvolution of the acquired images with the point spread function that describes the veiling glare, a concept that was further advanced by Close *et al.*[60] to account for spatial variability of the point spread function.

Geometric distortion introduced by the physics of the imaging system have been analyzed and corrected. Cerveri *et al.*[61] reported two techniques to correct geometric distortion introduced by image intensifiers, a local unwarping polynomial approach and a hierarchical radial basis function network (Fig. 6). Fantozzi *et al.*[62] developed a thin-plate-spline global-correction technique, while Yan *et al.*[65] presented an approach that incorporated a moving least squares method combined with polynomial fitting. These groups all conducted an array of evaluations and comparisons on simulated and real image data to assess the sensitivity of the various methods to specific distortions (e.g., pincushion, sigmoidal, and local distortion). In the context of magnetic resonance imaging (MRI), Sekihara and Kohno[57] presented an image restoration technique to overcome the effects of nonuniform static magnetic fields in modified echo-planar imaging, and Baldwin *et al.*[64] used a reversed gradient method to separate and correct geometric inaccuracies due to inhomogeneities in the background field and nonlinearities in the applied gradient. Zhang *et al.*[66] used deconvolution to restore the resolution of digital autoradiography images to improve the correlation of the radiotracer distribution in a tissue section with histology and immunohistochemistry findings.

V. NOISE REDUCTION

Most medical images are inherently noisy due to the desire to keep the radiation dose as low as possible or maintain short scan times. Techniques to reduce image noise and improve image contrast, therefore, have been the topic of numerous investigations. Buades *et al.*[67] provide an excellent overview of a wide range of popular denoising techniques.

A large number of such studies have been conducted in the context of radionuclide imaging. Webb *et al.*[55] described a constrained deconvolution approach applied to single-photon emission computed tomography (SPECT) images of the liver to improve cold-object contrast. Penny *et al.*[56] investigated an adaptive constrained least-squares method to perform planar image restoration (in terms of reduced noise and improved contrast) once the system MTF is known; subjective studies supported use of a "coarseness function" designed to minimize the energy in the second derivative of the

FIG. 6. (a) The correction grid along with (b) the original, distorted image from an image intensifier and (c) the image corrected with a local unwarping polynomial. (Reprinted with permission from Ref. 61.)

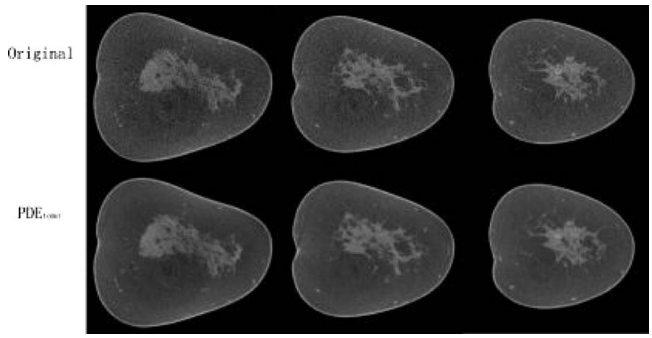

FIG. 7. The top row shows coronal sections from the CT scan of a normal breast. The bottom row shows the same sections after application of a dedicated noise removal algorithm. (Reprinted with permission from Ref. 71.)

restored image. This method was later extended to SPECT images.[58] A wavelet-based neural network filter was developed by Qian and Clarke[59] to reduce noise in gamma-camera imaging of beta-emitting isotopes required for the management of antibody therapy. Other areas where noise reduction is particularly important include dual-energy imaging[68,69] and low-dose computed tomography (CT);[70] noise reduction techniques developed in these areas are often modality specific and require access to the raw data.

Nonlinear diffusion schemes are extremely powerful for noise reduction in medical images. Xia *et al.*[71] used such techniques to improve the quality of breast CT images. Improved results were obtained when denoising was applied to the projection data rather than to reconstructed images (Fig. 7). A drawback of these schemes is their slow speed; therefore, other researchers have developed simpler techniques such as adaptive mean filtering,[72] the sigma filter,[73] and the SUSAN filter.[74] In the study by Hilts and Duzenli,[75] many such techniques were compared for performing dosimetry using polyacrylamide gels with CT. Schilham *et al.*[76] developed an extension of the SUSAN filter that adapts the filtering strength to local noise characteristics; emphysema scores of ultralow-dose CT scans subjected to this filter were similar to scores obtained from clinical-dose scans of the same patients.

VI. ENHANCED VISUALIZATION

Radiologists routinely interpret radiographic images along with previous images of the same patient for comparison to observe changes in anatomic structure or pathologic developments. An image processing technique known as temporal subtraction facilitates the visualization of pathologic change over a temporal sequence of patient images.[77–81] The resulting temporal subtraction images improve radiologists' ability to identify subtle focal lesions (e.g., lung cancers) and to recognize diffuse changes (Fig. 8).

Kano *et al.*[77] reported a temporal subtraction process for radiographic chest images based on small regions of interest automatically placed within the lung fields. A cross-correlation method and polynomial fitting were applied to determine shift values between the coordinates of the two images. Temporal subtraction images improved the detection

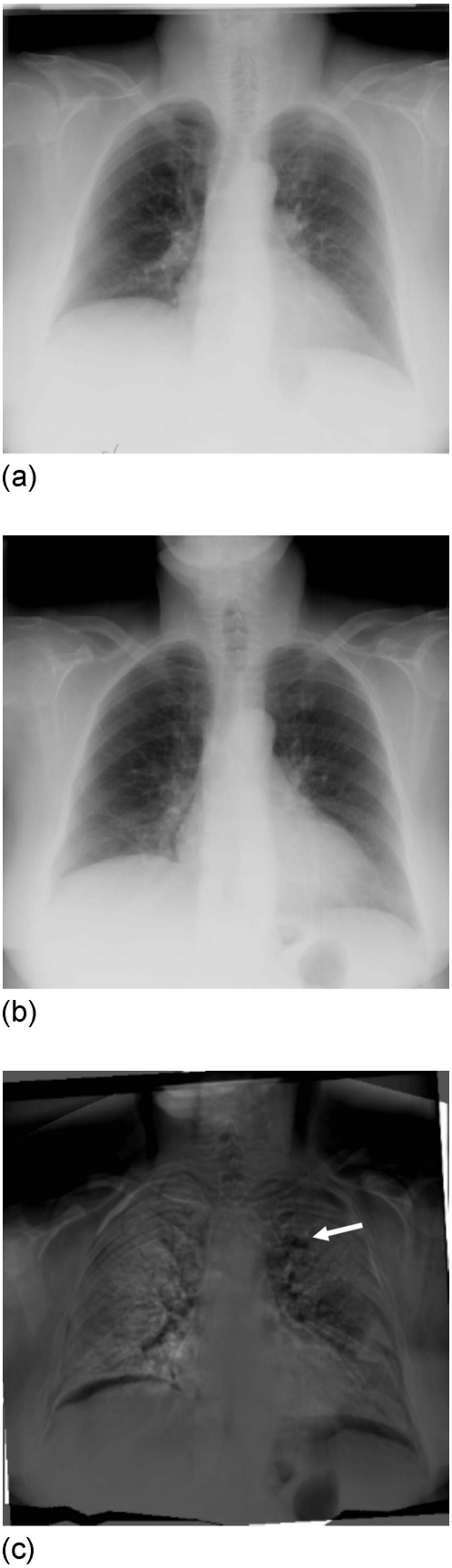

FIG. 8. Chest radiographs of the same patient acquired at different times. (a) Previous and (b) current images. (c) The temporal subtraction image clearly depicts change in the left upper lobe lung nodule (arrow). (Courtesy of H. MacMahon, M.D., The University of Chicago.)

of interval change in tumors and other opacities and assisted radiologists in the assessment of pleural effusions, heart size, air fluid levels, and pneumothoraces as they changed over time. Ishida *et al.*[78] improved the quality of subtraction images of the chest through an iterative warping approach. Armato *et al.*[82] later developed an automated approach to the evaluation of temporal subtraction image quality.

A temporal subtraction technique based on nonlinear warping was used by Shiraishi *et al.*[81] to create temporal subtraction images of radionuclide whole-body bone scans; these temporal subtraction images were used as part of a computerized scheme for the automated detection of interval change. Other investigators have developed methods to associate related structures in temporally sequential images without directly constructing a temporal subtraction image. For example, Hadjiiski *et al.*[79] and Timp *et al.*[80] developed regional registration methods to identify corresponding mass lesions in temporal pairs of mammograms.

Temporal subtraction methods typically define one image from the image pair as the mask image to which the other image is registered through some combination of global and local registration methods; the net effect is a spatial "warping" of the one image, which is then subtracted from the other image. Consequently, image registration algorithms provide the foundation for temporal subtraction. Image registration is itself a rich topic in medical image research, with significant contributions to the field made by medical physicists. A search for the term "image registration" in the title, abstract, or keywords of the 8166 articles indexed on the *Medical Physics* web site to-date yielded 214 hits that involve multimodality images,[83–86] atlas-based models,[87,88] two-view or bilateral comparisons,[89–92] radiotherapy patient setup,[93–97] respiratory motion correction,[98–104] and a wide variety of other applications.

Unlike temporal subtraction, which may be performed retrospectively on existing images through image manipulation and requires no alteration to the manner in which the radiographic images are acquired, energy subtraction (or dual-energy imaging) requires dedicated hardware to capture a "low-energy image" and a "high-energy image" of the patient during the same radiographic examination. These two images may be mathematically combined to create a pair of diagnostically distinct images, for example a "soft tissue image" predominantly depicting structures with attenuation close to that of water and a "bone image" predominantly depicting structures with attenuation close to that of calcium. Dual-energy imaging has been applied to breast imaging,[105] cardiac imaging,[106,107] chest imaging,[108,109] angiography,[110,111] and bone mineral content assessment.[112] In chest radiography, dual-energy imaging serves a two-fold role in the evaluation of lung cancer: first, the soft-tissue image eliminates superimposed bone that might obscure subtle lung nodules, and second, calcified nodules may be differentiated from noncalcified nodules, since only calcified nodules will appear on the bone image (Fig. 9). Armato *et al.*[113] used energy subtraction chest images as input to a temporal subtraction process to demonstrate the potential of these combined enhanced visualization techniques.

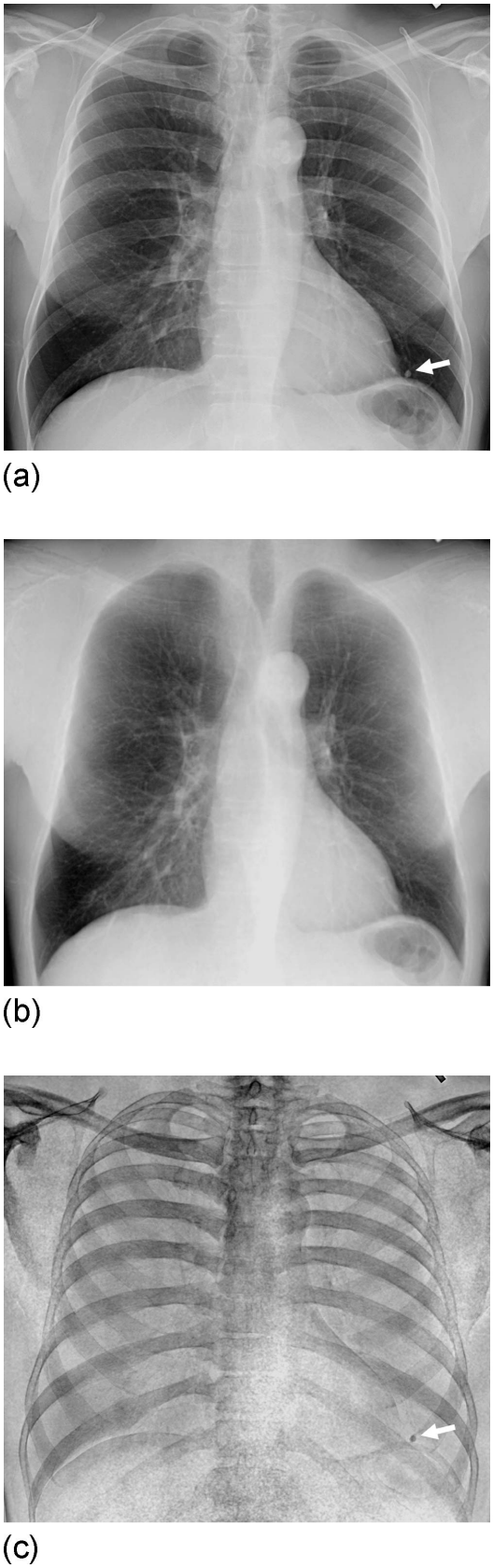

FIG. 9. Dual-energy chest radiography may be used to produce (a) a standard radiographic image, (b) a soft-tissue image, and (c) a bone image. The nodule demonstrated in the standard radiographic image (arrow) may be identified as a calcified granuloma since it appears in the bone image (arrow) but not the soft-tissue image. (Reprinted with permission from Ref. 164).

VII. IMAGE PREPROCESSING

A vast array of image preprocessing techniques has been developed and applied to medical images to achieve a wide range of results. The images generated by these preprocessing techniques may be used directly to attain some clinical benefit (for example, improved lesion conspicuity) or as input to higher level computer vision schemes, one prominent example of which is computer-aided diagnosis (CAD). Furthermore, a series of such techniques may be performed in an appropriate order to create more advanced preprocessing methods.

Image preprocessing techniques consist of operations designed to suppress image information not relevant to the specific task or to enhance key image features. Such techniques include unsharp masking,[114–117] global contrast enhancement,[115,116,118] histogram equalization,[119–121] edge enhancement,[122,123] and selective enhancement.[124] Loo *et al.*[114] used a statistical decision theory that incorporated the observer's visual transfer function to compute the signal-to-noise ratio of radiologic patterns after processing with an unsharp-masking technique. The calculated results agreed with qualitative results obtained from an observer performance study and demonstrated that unsharp masking improves the detectability of simple objects if parameters of the technique are selected properly. Brailean *et al.*[118] used similar statistical decision theory to demonstrate the superiority of an expectation maximization algorithm over global contrast enhancement and unsharp masking for the enhancement of small objects in radiographic images. Global contrast enhancement and unsharp masking applied to computed radiography (CR) portal images were found by Wilenzick and Merritt[115] to generate images at least as good as the best portal films obtained with then-conventional commercial radiotherapy screen-film systems. Weiser *et al.*[116] demonstrated a statistical improvement in the perception of anatomic detail for similarly preprocessed CR portal images. Stahl *et al.*[117] extended the concept of unsharp masking to a multiscale architecture that hierarchically enhanced structures over a range of sizes (Fig. 10).

Kim *et al.*[120] evaluated the impact of image preprocessing techniques such as global contrast enhancement and histogram equalization on a rigid three-dimensional/two-dimensional registration method. Histogram equalization was found to be a key preprocessing step for accurate registration. Histogram equalization was used by Lehmann *et al.*[121] to increase the sharpness of coronary arteries prior to application of an image-based metric for measuring the extent of motion in angiographic images and by Crooks and Fallone[119] to improve visualization of double-exposure portal images and facilitate the beam verification process.

Edges are key features in medical images as they provide visual cues for structure boundaries, fine textural detail, and many pathologic processes. Consequently, image processing techniques that enhance edges have a prominent role in diagnostic radiology and radiation oncology. Leszczynski *et al.*[122] developed an edge extraction algorithm to delineate the treatment field in portal images; their method was based on a

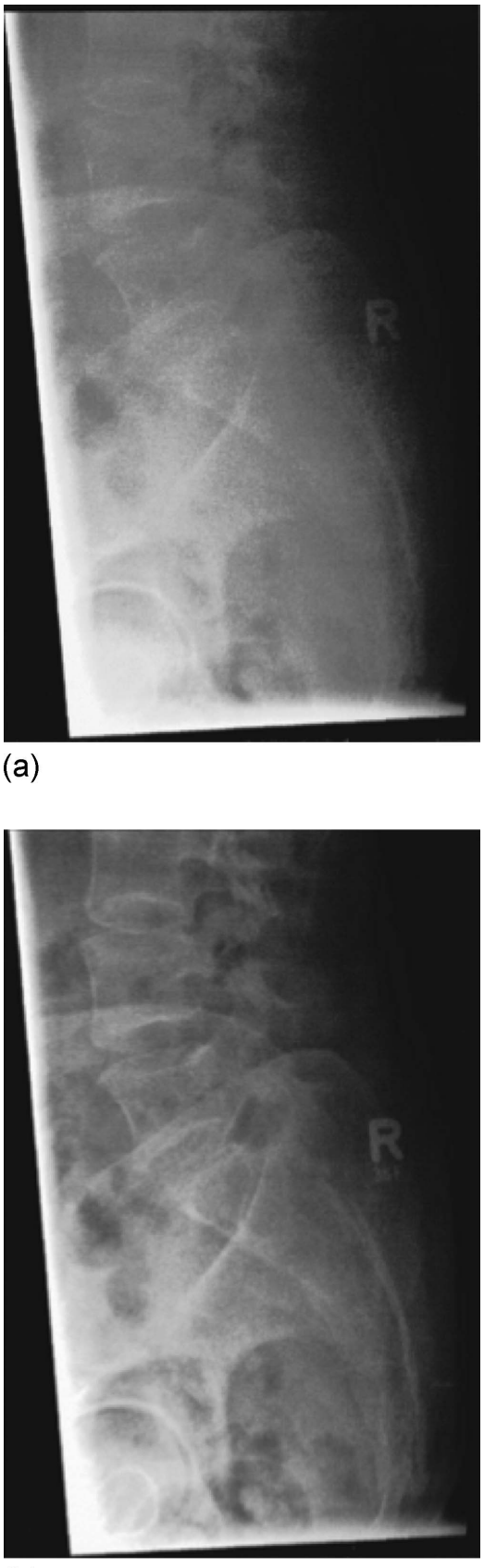

FIG. 10. Radiographic image of the sacrum processed (a) with a standard unsharp-masking algorithm and (b) with a multiscale algorithm for the hierarchical enhancement of structures. (Reprinted with permission from Ref. 117.)

derivative of Gaussian operator. Crooks and Fallone[123] used local histogram analysis to create a general edge enhancement algorithm that did not also substantially enhance image noise. The enhancement (and subsequent detection) of edges is an essential component of many image segmentation techniques and an important preprocessing step for a variety of CAD applications.[125,126]

VIII. SEGMENTATION

Segmentation is a holy grail in computer vision and one of the most widely studied subjects in medical image processing. Segmentation is often a prerequisite for compound analysis systems, such as CAD applications. Consequently, many segmentation techniques have been reported for the structures and organs of interest in the major areas of CAD research, such as breast, lung, and colon. A complete overview of CAD applications that incorporate segmentation is comprehensively reviewed in the Anniversary Paper by Giger *et al.*[127]

Image segmentation is crucial for accurate planning of radiotherapy, and the large number of such procedures makes it likely that segmentation is performed more often as a clinical procedure in radiation oncology than in all other medical specialties combined.[128] Consequently, a large body of work is devoted to segmentation for the purpose of radiotherapy treatment. On segmentation of the prostate alone, ten studies have appeared in *Medical Physics* since 2000, mainly focusing on two- and three-dimensional ultrasound, but more recently also on CT and MRI. A recent Point/Counterpoint article debated whether segmentation methods for radiation therapy treatment planning should be standardized and calibrated,[128] an issue that is important for all applications of medical image segmentation.

The segmentation of organs and lesions is essential for many image-based quantification tasks. Duryea *et al.*[129] used semiautomated segmentation tools to measure the joint destruction on wrist CT scans from patients with rheumatoid arthritis. Hardisty *et al.*[130] analyzed bone metastases by segmenting the vertebral body and the trabecular centrum of tumor-involved and healthy vertebrae. Zhuge *et al.*[131] segmented aortic aneurysms in CT angiograms to measure volume and morphological aspects useful for treatment planning. Angelie *et al.*[132] segmented the left ventricular (LV) myocardial borders in cardiovascular MR to measure LV function parameters such as the ejection fraction and wall motion. Mao *et al.*[133] and Gill *et al.*[134] extracted the carotid arteries from ultrasound images to estimate the degree of stenosis. Yuan *et al.*[135] developed a two-stage approach to the segmentation of mass lesions on digital mammograms, and Horsch *et al.*[136] segmented mass lesions on breast ultrasound images. Some topics have attracted a large amount of research because of their evident clinical importance. Examples include the segmentation of lung nodules from thoracic CT scans[137–139] and the segmentation of tumors from PET scans.[140–143] These examples demonstrate the wide range of applications for segmentation-based quantification.

A segmentation result may be used as input for fast and effective visualization by volume or surface rendering algorithms. Manual editing of cutplanes is one of the most time-consuming aspects of volume rendered displays, which are used increasingly in clinical practice. Over the last few years, commercial vendors have integrated into their workstations automated segmentation tools that provide at least an approximate location of structures of interest. Interestingly, high-precision segmentations often are not required for this purpose; a rough delineation of a volume of interest usually suffices, but it is advantageous to remove, for example, the sternum in a volume rendering of the heart.

Methodologically, segmentation methods have shifted from rule-based systems to supervised approaches that learn a model of the object to be segmented. Model attributes may include object size, shape, location in an image (either absolute or relative to other structures), and appearance. For model-based approaches, training data consisting of images with the desired segmentations are required to train the system. The test phase, in which a previously unseen image is segmented, can be viewed as fitting the precomputed model to the novel image. Popular examples of such approaches include active shape models,[144] active appearance models,[145] and *m*-reps.[146] Many methods that employ pixel labeling are also supervised, although such methods do not contain an explicit model of the shape of the object to be segmented.

A good illustration of this shift is the segmentation of lung fields in chest radiographs. Several groups have presented rule-based techniques to achieve lung segmentation.[147–150] These methods are representative of many others, published in the 1980s and 1990s, that employ sequences of classic image processing techniques to arrive at a segmentation. The "art" of developing such methods is to choose appropriate combinations of techniques and proper values for the many parameters that govern the behavior of the method. Pixel labeling also has been used for lung field segmentation,[151–153] and more recent studies in this area invariably use supervised methods.[154–156]

A major advantage of these supervised methods is that, theoretically, they are applicable to many different tasks, provided that suitable sets of training images are available. In practice, however, many of these methods require changes and adjustments for particular applications. This is the topic of many recent publications. Pilgram *et al.*,[157] for example, presented several modifications to active shape models to allow application of these models to proximal femur segmentation in pelvic radiographs. It should be noted that rule-based schemes, both automated and semiautomated, are still being developed for situations where clinical practice requires fast algorithms, such as in the recent work of Bekes *et al.*;[158] another nonsupervised methodology that has attracted much attention is level sets, used, for example, by Zhuge *et al.*[159] to prevent boundary leakage through poorly resolved edges.

Atlas-based segmentation uses the paradigm of interpatient registration for the purpose of segmentation: by registering a novel image to a reference image with known segmentation (the atlas), the obtained transformation can be

applied to the segmentation (label propagation) to yield a segmentation of the novel image. The general applicability of this methodology is its major attraction. The number of applications and possible variations on the basic approach is large.[87,88]

Finally, we note the recent interest in segmentation strategies for the analysis of four-dimensional (three spatial dimensions plus time) images.[160–163] Due to the everincreasing capabilities of modern scanners, this trend toward four-dimensional image acquisition certainly will continue. The challenges for investigators developing appropriate image segmentation tools will continue as well.

IX. SUMMARY

The shift from the radiographic film to the radiographic image has both allowed and necessitated numerous developments in image processing and manipulation to achieve image restoration, noise reduction, enhanced visualization, image registration, preprocessing for improved structure visualization, and image segmentation. These techniques are themselves powerful as individual applications while providing tremendous benefits as components of advanced computer vision methods. This shift has been accompanied by challenges in image display and image informatics. These challenges and developments all have been actively advanced by medical physicists and the AAPM through the pages of *Medical Physics*.

[a]Author to whom correspondence should be addressed. Telephone: 773-834-3044; Fax: 773-702-0371. Electronic mail: s-armato@uchicago.edu

[1]A. G. Haus, J. E. Gray, and T. R. Daly, "Evaluation of mammographic viewbox luminance, illuminance, and color," Med. Phys. **20**, 819–821 (1993).
[2]A. S. Chawla and E. Samei, "Ambient illumination revisited: A new adaptation-based approach for optimizing medical imaging reading environments," Med. Phys. **34**, 81–90 (2007).
[3]W. D. Renner and J. C. Luke, "Image processing of conventional tomograms," Med. Phys. **8**, 388–395 (1981).
[4]J. C. Weiser, D. Gur, R. C. Gennari, and M. Deutsch, "Evaluation of analog contrast enhancement and digital unsharp masking in low-contrast portal images," Med. Phys. **17**, 122–125 (1990).
[5]H. Liu, J. Xu, L. L. Fajardo, S. Yin, and F. T. S. Yu, "Optical processing architecture and its potential application for digital and analog radiography," Med. Phys. **26**, 648–652 (1999).
[6]A. Panchangam, K. V. L. N. Sastry, D. V. G. L. N. Rao, B. S. DeCristofano, B. R. Kimball, and M. Nakashima, "Processing of medical images using real-time optical Fourier processing," Med. Phys. **28**, 22–27 (2001).
[7]T. Villafana, "Modulation transfer function of a finite scanning microdensitometer slit," Med. Phys. **2**, 251–254 (1975).
[8]F.-F. Yin, M. L. Giger, and K. Doi, "Measurement of the presampling modulation transfer function of film digitizers using a curve fitting technique," Med. Phys. **17**, 962–966 (1990).
[9]H. Yoshimura, X.-W. Xu, K. Doi, H. MacMahon, K. R. Hoffmann, M. L. Giger, and S. M. Montner, "Development of a high quality film duplication system using a laser digitizer: Comparison with computed radiography," Med. Phys. **20**, 51–58 (1993).
[10]R. J. J. Meeder, D. A. Jaffray, and P. Munro, "Tests for evaluating laser film digitizers," Med. Phys. **22**, 635–642 (1995).
[11]N. J. Hangiandreou, T. J. O'Connor, and J. P. Felmlee, "An evaluation of the signal and noise characteristics of four CCD-based film digitizers," Med. Phys. **25**, 2020–2026 (1998).
[12]J. F. Dempsey, D. A. Low, A. S. Kirov, and J. F. Williamson, "Quantitative optical densitometry with scanning-laser film digitizers," Med. Phys. **26**, 1721–1731 (1999).
[13]A. González, J. A. Martínez, and B. Tobarra, "Technical note: Signal resolution increase and noise reduction in a CCD digitizer," Med. Phys. **31**, 525–527 (2004).
[14]G. R. Gluckman and L. E. Reinstein, "Comparison of three high-resolution digitizers for radiochromic film dosimetry," Med. Phys. **29**, 1839–1846 (2002).
[15]S. Devic, J. Seuntjens, G. Hegyi, E. B. Podgorsak, C. G. Soares, A. S. Kirov, I. Ali, J. F. Williamson, and A. Elizondo, "Dosimetric properties of improved GafChromic films for seven different digitizers," Med. Phys. **31**, 2392–2401 (2004).
[16]E. Wilcox, G. Daskalov, and L. Nedialkova, "Comparison of the Epson Expression 1680 flatbed and the Vidar VXR-16 Dosimetry PRO film scanners for use in IMRT dosimetry using Gafchromic and radiographic film," Med. Phys. **34**, 41–48 (2007).
[17]P. G. Nagy, "The future of PACS," Med. Phys. **34**, 2676–2682 (2007).
[18]J. H. Trueblood, K. R. Hogstrom, and W. R. Hendee, "Medical physicists should position themselves as institutional resources in expanding areas such as healthcare informatics and information networking," Med. Phys. **27**, 631–633 (2000).
[19]J. R. Halama, W. Huda, and W. R. Hendee, "Medical physicists should assume PACS responsibilities," Med. Phys. **29**, 1913–1915 (2002).
[20]G. C. Nikiforidis, G. C. Kagadis, and C. G. Orton, "It is important that medical physicists be involved in the development and implementation of integrated hospital information systems," Med. Phys. **33**, 4455–4458 (2006).
[21]G. C. Kagadis, P. Nagy, S. Langer, M. Flynn, and G. Starkschall, "Anniversary Paper: Roles of medical physicists and health care applications of informatics," Med. Phys. **35**, 119–127 (2008).
[22]B. S. Baxter, L. E. Hitchner, and G. Q. Maquire, Jr., *AAPM Report No. 10: A Standard Format for Digital Image Exchange* (American Institute of Physics, New York, 1982).
[23]J. Morishita, S. Katsuragawa, K. Kondo, and K. Doi, "An automated patient recognition method based on an image-matching technique using previous chest radiographs in the picture archiving and communication system environment," Med. Phys. **28**, 1093–1097 (2001).
[24]H. Arimura, S. Katsuragawa, Q. Li, T. Ishida, and K. Doi, "Development of a computerized method for identifying the posteroanterior and lateral views of chest radiographs by use of a template matching technique," Med. Phys. **29**, 1556–1561 (2002).
[25]K. H. Höhne, U. Obermöller, M. Riemer, G. Witte, and M. Böhm, "Data compression in digital angiography using the Fourier transform," Med. Phys. **10**, 899–905 (1983).
[26]J. Liénard, "Real-time distortionless high-factor compression scheme," Med. Phys. **16**, 845–850 (1989).
[27]S.-C. B. Lo, E. L. Shen, S. K. Mun, and J. Chen, "A method for splitting digital value in radiological image compression," Med. Phys. **18**, 939–946 (1991).
[28]L. T. Cook, M. F. Insana, M. A. McFadden, T. J. Hall, and G. G. Cox, "Contrast-detail analysis of image degradation due to lossy compression," Med. Phys. **22**, 715–721 (1995).
[29]G. G. Cox, L. T. Cook, M. F. Insana, M. A. McFadden, T. J. Hall, L. A. Harrison, D. A. Eckard, and N. L. Martin, "The effects of lossy compression on the detection of subtle pulmonary nodules," Med. Phys. **23**, 127–132 (1996).
[30]F.-F. Yin and Q. Gao, "Oncologic image compression using both wavelet and masking techniques," Med. Phys. **24**, 2038–2042 (1997).
[31]B. Zhao, L. H. Schwarz, and P. K. Kijewski, "Effects of lossy compression on lesion detection: Predictions of the nonprewhitening matched filter," Med. Phys. **25**, 1621–1624 (1998).
[32]N. C. Phelan and J. T. Ennis, "Medical image compression based on a morphological representation of wavelet coefficient," Med. Phys. **26**, 1607–1611 (1999).
[33]S. K. Thompson, J. D. Hazle, D. F. Schomer, A. A. Elekes, D. A. Johnston, J. Huffman, and C. K. Chui, "Performance analysis of a new semiorthogonal spline wavelet compression algorithm for tonal medical images," Med. Phys. **27**, 276–288 (2000).
[34]A. Fidler, U. Skaleric, and B. Likar, "The impact of image information on compressibility and degradation in medical image compression," Med. Phys. **33**, 2832–2838 (2006).
[35]P. D. Esser and R. A. Fawwaz, "A spatially calibrated computer display and associated quality assurance," Med. Phys. **7**, 168 (1980).
[36]F. G. Sommer, S. C. Orphanoudakis, and K. J. W. Taylor, "Preliminary evaluation of display format effects on perceptibility in a low contrast ultrasound test object," Med. Phys. **8**, 155–157 (1981).

[37]M. L. Giger, K. Ohara, and K. Doi, "Investigation of basic imaging properties in digital radiography. 9. Effect of displayed grey levels on signal detection," Med. Phys. **13**, 312–318 (1986).
[38]R. D. Nawfel, K. H. Chan, D. J. Wagenaar, and P. F. Judy, "Evaluation of video gray-scale display," Med. Phys. **19**, 561–567 (1992).
[39]J. Moseley and P. Munro, "Display equalization: A new display method for portal images," Med. Phys. **20**, 99–102 (1993).
[40]L. T. Cook, G. G. Cox, M. F. Insana, M. A. McFadden, T. J. Hall, R. S. Gaborski, and F. Y. M. Lure, "Comparison of a cathode-ray-tube and film for display of computed radiographic images," Med. Phys. **25**, 1132–1138 (1998).
[41]B. M. Hemminger, A. W. Dillon, R. E. Johnston, K. E. Muller, M. C. Deluca, C. S. Coffey, and E. D. Pisano, "Effect of display luminance on the feature detection rates of masses in mammograms," Med. Phys. **26**, 2266–2272 (1999).
[42]A. Badano, M. J. Flynn, S. Martin, and J. Kanicki, "Angular dependence of the luminance and contrast in medical monochrome liquid crystal displays," Med. Phys. **30**, 2602–2613 (2003).
[43]A. Badano and D. H. Fifadara, "Goniometric and conoscopic measurements of angular display contrast for one-, three-, five-, and nine-million-pixel medical liquid crystal displays," Med. Phys. **31**, 3452–3460 (2004).
[44]A. Badano, R. M. Gagne, R. J. Jennings, S. E. Drilling, B. R. Imhoff, and E. Muka, "Noise in flat-panel displays with subpixel structure," Med. Phys. **31**, 715–723 (2004).
[45]H. Jung, H.-J. Kim, W.-S. Kang, S. K. Yoo, K. Fujioka, M. Hasegawa, and E. Samei, "Assessment of flat panel LCD primary class display performance based on AAPM TG 18 acceptance protocol," Med. Phys. **31**, 2155–2164 (2004).
[46]E. Samei, A. Badano, D. Chakraborty, K. Compton, C. Cornelius, K. Corrigan, M. J. Flynn, B. Hemminger, N. Hangiandreou, J. Johnson, D. M. Moxley-Stevens, W. Pavlicek, H. Roehrig, L. Rutz, S. J. Shepard, R. A. Uzenoff, J. Wang, and C. E. Willis, "Assessment of display performance for medical imaging systems: Executive summary of AAPM TG18 report," Med. Phys. **32**, 1205–1225 (2005).
[47]E. Samei, A. Badano, D. Chakraborty, K. Compton, C. Cornelius, K. Corrigan, M. J. Flynn, B. Hemminger, N. Hangiandreou, J. Johnson, D. M. Moxley-Stevens, W. Pavlicek, H. Roehrig, L. Rutz, S. J. Shepard, R. A. Uzenoff, J. Wang, and C. E. Willis, AAPM On-Line Report No. 03: Assessment of Display Performance for Medical Imaging Systems, 2005.
[48]E. Samei and S. L. Wright, "Viewing angle performance of medical liquid crystal displays," Med. Phys. **33**, 645–654 (2006).
[49]R. S. Saunders, Jr. and E. Samei, "Resolution and noise measurements of five CRT and LCD medical displays," Med. Phys. **33**, 308–319 (2006).
[50]J. Jacobs, F. Rogge, J. Kotre, G. Marchal, and H. Bosmans, "Preliminary validation of a new variable pattern for daily quality assurance of medical image display devices," Med. Phys. **34**, 2744–2758 (2007).
[51]H. Liang and A. Badano, "Temporal response of medical liquid crystal displays," Med. Phys. **34**, 639–646 (2007).
[52]E. Samei, N. T. Ranger, and D. M. Delong, "A comparative contrast-detail study of five medical displays," Med. Phys. **35**, 1358–1364 (2008).
[53]*AAPM Report No. 42. The Role of the Clinical Medical Physicist in Diagnostic Radiology, Report of the AAPM Task Group No. 2* (American Institute of Physics, Woodbury, NY, 1994).
[54]J. A. Seibert, O. Nalcioglu, and W. Roeck, "Removal of image intensifier veiling glare by mathematical deconvolution techniques," Med. Phys. **12**, 281–288 (1985).
[55]S. Webb, A. P. Long, R. J. Ott, M. O. Leach, and M. A. Flower, "Constrained deconvolution of SPECT liver tomograms by direct digital image restoration," Med. Phys. **12**, 53–58 (1985).
[56]B. C. Penney, M. A. King, R. B. Schwinger, S. P. Baker, P. Stritzke, and P. W. Doherty, "Constrained least-squares restoration of nuclear medicine images: Selecting the coarseness function," Med. Phys. **14**, 849–858 (1987).
[57]K. Sekihara and H. Kohno, "Image restoration from nonuniform static field influence in modified echo-planar imaging," Med. Phys. **14**, 1087–1089 (1987).
[58]B. C. Penney, M. A. King, and R. B. Schwinger, "Modifying constrained least-squares restoration for application to single photon emission computed tomography projection images," Med. Phys. **15**, 334–342 (1988).
[59]W. Qian and L. P. Clarke, "A restoration algorithm for P-32 and Y-90 bremsstrahlung emission nuclear imaging: A wavelet-neural network approach," Med. Phys. **23**, 1309–1323 (1996).
[60]R. A. Close, K. C. Shah, and J. S. Whiting, "Regularization method for scatter-glare correction in fluoroscopic images," Med. Phys. **26**, 1794–1801 (1999).
[61]P. Cerveri, C. Forlani, N. A. Borghese, and G. Ferrigno, "Distortion correction for x-ray image intensifiers: Local unwarping polynomials and RBF neural networks," Med. Phys. **29**, 1759–1771 (2002).
[62]S. Fantozzi, A. Cappello, and A. Leardini, "A global method based on thin-plate splines for correction of geometric distortion: An application to fluoroscopic images," Med. Phys. **30**, 124–131 (2003).
[63]D. W. Holdsworth, S. I. Pollmann, H. N. Nikolov, and R. Fahrig, "Correction of XRII geometric distortion using a liquid-filled grid and image subtraction," Med. Phys. **32**, 55–64 (2005).
[64]L. N. Baldwin, K. Wachowicz, S. D. Thomas, R. Rivest, and B. G. Fallone, "Characterization, prediction, and correction of geometric distortion in 3 TMR images," Med. Phys. **34**, 388–399 (2007).
[65]S. Yan, C. Wang, and M. Ye, "A method based on moving least squares for XRII image distortion correction," Med. Phys. **34**, 4194–4206 (2007).
[66]M. Zhang, Q. Chen, X.-F. Li, J. O'Donoghue, S. Ruan, P. Zanzonico, C. C. Ling, and J. L. Humm, "Image deconvolution in digital autoradiography: A preliminary study," Med. Phys. **35**, 522–530 (2008).
[67]A. Buades, B. Coll, and J. Morel, "A review of image denoising algorithms, with a new one," Multiscale Model. Simul. **4**, 490–530 (2005).
[68]R. J. Warp and J. T. Dobbins III, "Quantitative evaluation of noise reduction strategies in dual-energy imaging," Med. Phys. **32**, 190–198 (2003).
[69]S. Richard and J. H. Siewerdsen, "Cascaded systems analysis of noise reduction algorithms in dual-energy imaging," Med. Phys. **35**, 586–601 (2008).
[70]P. J. La Rivière, "Penalized-likelihood sinogram smoothing for low-dose CT," Med. Phys. **32**, 1676–1683 (2005).
[71]J. Q. Xia, J. Y. Lo, K. Yang, C. E. Floyd, Jr., and J. M. Boone, "Dedicated breast computed tomography: Volume image denoising via a partial-diffusion equation based technique," Med. Phys. **35**, 1950–1958 (2008).
[72]M. Hilts and A. Jirasek, "Adaptive mean filtering for noise reduction in CT polymer gel dosimetry," Med. Phys. **35**, 344–355 (2008).
[73]J.-S. Lee, "Digital image smoothing and the sigma filter," Comput. Vis. Graph. Image Process. **24**, 255–269 (1998).
[74]S. Smith and J. Brady, "SUSAN—a new approach to low level image processing," Int. J. Comput. Vis. **23**, 45–78 (1997).
[75]M. Hilts and C. Duzenli, "Image filtering for improved dose resolution in CT polymer gel dosimetry," Med. Phys. **31**, 39–49 (2004).
[76]A. Schilham, B. van Ginneken, H. Gietema, and M. Prokop, "Local noise weighted filtering for emphysema scoring of low-dose CT images," IEEE Trans. Med. Imaging **25**, 451–463 (2006).
[77]A. Kano, K. Doi, H. MacMahon, D. D. Hassell, and M. L. Giger, "Digital image subtraction of temporally sequential chest images for detection of interval change," Med. Phys. **21**, 453–461 (1994).
[78]T. Ishida, S. Katsuragawa, K. Nakamura, H. MacMahon, and K. Doi, "Iterative image warping technique for temporal subtraction of sequential chest radiographs to detect interval change," Med. Phys. **26**, 1320–1329 (1999).
[79]L. Hadjiiski, H.-P. Chan, B. Sahiner, N. Petrick, and M. A. Helvie, "Automated registration of breast lesions in temporal pairs of mammograms for interval change analysis—Local affine transformation for improved localization," Med. Phys. **28**, 1070–1079 (2001).
[80]S. Timp, S. van Engeland, and N. Karssemeijer, "A regional registration method to find corresponding mass lesions in temporal mammogram pairs," Med. Phys. **32**, 2629–2638 (2005).
[81]J. Shiraishi, Q. Li, D. Appelbaum, Y. Pu, and K. Doi, "Development of a computer-aided diagnostic scheme for detection of interval changes in successive whole-body bone scans," Med. Phys. **34**, 25–36 (2007).
[82]S. G. Armato III, D. J. Doshi, R. Engelmann, C. L. Croteau, and H. MacMahon, "Temporal subtraction in chest radiography: Automated assessment of registration accuracy," Med. Phys. **33**, 1239–1249 (2006).
[83]Q.-S. Chen, M. Defrise, and F. Deconinck, "Three-dimensional multimodality medical image registration using a parameter accumulation approach," Med. Phys. **23**, 877–885 (1996).
[84]E. E. Graves, A. Pirzkall, S. J. Nelson, D. Larson, and L. Verhey, "Registration of magnetic resonance spectroscopic imaging to computed tomography for radiotherapy treatment planning," Med. Phys. **28**, 2489–2496 (2001).
[85]G. C. Kagadis, K. K. Delibasis, G. K. Matsopoulos, N. A. Mouravliansky, P. A. Asvestas, and G. C. Nikiforidis, "A comparative study of surface- and volume-based techniques for the automatic registration between CT and SPECT brain images," Med. Phys. **29**, 201–213 (2002).

[86]M. Söhn, M. Birkner, Y. Chi, J. Wang, D. Yan, B. Berger, and M. Alber, "Model-independent, multimodality deformable image registration by local matching of anatomical features and minimization of elastic energy," Med. Phys. **35**, 866–878 (2008).
[87]J. Stancanello, P. Romanelli, N. Modugno, P. Cerveri, G. Ferrigno, F. Uggeri, and G. Cantore, "Atlas-based identification of targets for functional radiosurgery," Med. Phys. **33**, 1603–1611 (2006).
[88]S. Klein, U. A. van der Heide, I. M. Lips, M. van Vulpen, M. Staring, and J. P. W. Pluim, "Automatic segmentation of the prostate in 3D MR images by atlas matching using localized mutual information," Med. Phys. **35**, 1407–1417 (2008).
[89]F.-F. Yin, M. L. Giger, K. Doi, C. J. Vyborny, and R. A. Schmidt, "Computerized detection of masses in digital mammograms: Automated alignment of breast images and its effect on bilateral-subtraction technique," Med. Phys. **21**, 445–452 (1994).
[90]Q. Li, S. Katsuragawa, T. Ishida, H. Yoshida, S. Tsukuda, H. MacMahon, and K. Doi, "Contralateral subtraction: A novel technique for detection of asymmetric abnormalities on digital chest radiographs," Med. Phys. **27**, 47–55 (2000).
[91]Y.-T. Wu, J. Wei, L. M. Hadjiiski, B. Sahiner, C. Zhou, J. Ge, J. Shi, Y. Zhang, and H.-P. Chan, "Bilateral analysis based false positive reduction for computer-aided mass detection," Med. Phys. **34**, 3334–3344 (2007).
[92]J. Pu, B. Zheng, J. K. Leader, and D. Gur, "An ellipse-fitting based method for efficient registration of breast masses on two mammographic views," Med. Phys. **35**, 487–494 (2008).
[93]J. Cai, J. C. H. Chu, V. A. Saxena, and L. H. Lanzl, "A simple algorithm for planar image registration in radiation therapy," Med. Phys. **25**, 824–829 (1998).
[94]A. E. Lujan, J. M. Balter, and R. K. T. Haken, "Determination of rotations in three dimensions using two-dimensional portal image registration," Med. Phys. **25**, 703–708 (1998).
[95]J. Kreß, S. Minohara, M. Endo, J. Debus, and T. Kanai, "Patient position verification using CT images," Med. Phys. **26**, 941–948 (1999).
[96]C. Bert, K. G. Metheany, K. Doppke, and G. T. Y. Chen, "A phantom evaluation of a stereo-vision surface imaging system for radiotherapy patient setup," Med. Phys. **32**, 2753–2762 (2005).
[97]J. Chang, K. M. Yenice, A. Narayana, and P. H. Gutin, "Accuracy and feasibility of cone-beam computed tomography for stereotactic radiosurgery setup," Med. Phys. **34**, 2077–2084 (2007).
[98]M. M. Coselmon, J. M. Balter, D. L. McShan, and M. L. Kessler, "Mutual information based CT registration of the lung at exhale and inhale breathing states using thin-plate splines," Med. Phys. **31**, 2942–2948 (2004).
[99]T. Pan, T.-Y. Lee, E. Rietzel, and G. T. Y. Chen, "4D-CT imaging of a volume influenced by respiratory motion on multi-slice CT," Med. Phys. **31**, 333–340 (2004).
[100]R. Tanaka, S. Sanada, M. Suzuki, T. Kobayashi, T. Matsui, H. Inoue, and N. Yoshihisa, "Breathing chest radiography using a dynamic flat-panel detector combined with computer analysis," Med. Phys. **31**, 2254–2262 (2004).
[101]K. Berlinger, M. Roth, O. Sauer, L. Vences, and A. Schweikard, "Fully automatic detection of corresponding anatomical landmarks in volume scans of different respiratory state," Med. Phys. **33**, 1569–1572 (2006).
[102]B. Thorndyke, E. Schreibmann, A. Koong, and L. Xing, "Reducing respiratory motion artifacts in positron emission tomography through retrospective stacking," Med. Phys. **33**, 2632–2641 (2006).
[103]Q. Zhang, A. Pevsner, A. Hertanto, Y.-C. Hu, K. E. Rosenzweig, C. C. Ling, and G. S. Mageras, "A patient-specific respiratory model of anatomical motion for radiation treatment planning," Med. Phys. **34**, 4772–4781 (2007).
[104]V. Boldea, G. C. Sharp, S. B. Jiang, and D. Sarrut, "4D-CT lung motion estimation with deformable registration: Quantification of motion nonlinearity and hysteresis," Med. Phys. **35**, 1008–1018 (2008).
[105]P. C. Johns, D. J. Drost, M. J. Yaffe, and A. Fenster, "Dual-energy mammography: Initial experimental results," Med. Phys. **12**, 297–304 (1985).
[106]S. Y. Molloi and C. A. Mistretta, "Quantification techniques for dual-energy cardiac imaging," Med. Phys. **16**, 209–217 (1989).
[107]T. Xu, J. L. Ducote, J. T. Wong, and S. Molloi, "Feasibility of real time dual-energy imaging based on a flat panel detector for coronary artery calcium quantification," Med. Phys. **33**, 1612–1622 (2006).
[108]J.-T. Ho, R. A. Kruger, and J. A. Sorenson, "Comparison of dual and single exposure techniques in dual-energy chest radiography," Med. Phys. **16**, 202–208 (1989).
[109]N. A. Shkumat, J. H. Siewerdsen, A. C. Dhanantwari, D. B. Williams, S. Richard, N. S. Paul, J. Yorkston, and R. Van Metter, "Optimization of image acquisition techniques for dual-energy imaging of the chest," Med. Phys. **34**, 3904–3915 (2007).
[110]J. Liu, D. Nishimura, and A. Macovski, "Vessel imaging using dual-energy tomosynthesis," Med. Phys. **14**, 950–955 (1987).
[111]M. S. Van Lysel, "Optimization of beam parameters for dual-energy digital subtraction angiography," Med. Phys. **21**, 219–226 (1994).
[112]R. A. Kruger, "Dual-energy electronic scanning-slit fluorography for the determination of vertebral bone mineral content," Med. Phys. **14**, 562–566 (1987).
[113]S. G. Armato III, D. J. Doshi, R. Engelmann, P. Caligiuri, and H. MacMahon, "Temporal subtraction of dual-energy chest radiographs," Med. Phys. **33**, 1911–1919 (2006).
[114]L.-N. D. Loo, K. Doi, and C. E. Metz, "Investigation of basic imaging properties in digital radiography. 4. Effect of unsharp masking on the detectability of simple patterns," Med. Phys. **12**, 209–214 (1985).
[115]R. M. Wilenzick and C. R. B. Merritt, "Megavoltage portal films using computed radiographic imaging with photostimulable phosphors," Med. Phys. **14**, 389–392 (1987).
[116]J. C. Weiser, D. Gur, and R. C. Gennari, "Evaluation of analog contrast enhancement and digital unsharp masking in low-contrast portal images," Med. Phys. **17**, 122–125 (1990).
[117]M. Stahl, T. Aach, and S. Dippe, "Digital radiography enhancement by nonlinear multiscale processing," Med. Phys. **27**, 56–65 (2000).
[118]J. C. Brailean, D. Little, M. L. Giger, C.-T. Chen, and B. J. Sullivan, "Application of the EM algorithm to radiographic images," Med. Phys. **19**, 1175–1182 (1992).
[119]I. Crooks and B. G. Fallone, "Contrast enhancement of portal images by selective histogram equalization," Med. Phys. **20**, 199–204 (1993).
[120]J. Kim, F.-F. Yin, Y. Zhao, and J. H. Kim, "Effects of x-ray and CT image enhancements on the robustness and accuracy of a rigid 3D/2D image registration," Med. Phys. **32**, 866–873 (2005).
[121]G. C. Lehmann, D. W. Holdsworth, and M. Drangova, "Angle-independent measure of motion for image-based gating in 3D coronary angiography," Med. Phys. **33**, 1311–1320 (2006).
[122]K. W. Leszczynski, S. Shalev, and N. S. Cosby, "The enhancement of radiotherapy verification images by an automated edge detection technique," Med. Phys. **19**, 611–621 (1992).
[123]I. Crooks and B. G. Fallone, "A novel algorithm for the edge detection and edge enhancement of medical images," Med. Phys. **20**, 993–998 (1993).
[124]Q. Li, S. Sone, and K. Doi, "Selective enhancement filters for nodules, vessels, and airway walls in two- and three-dimensional CT scans," Med. Phys. **30**, 2040–2051 (2003).
[125]T. Ema, K. Doi, R. M. Nishikawa, Y. Jiang, and J. Papaioannou, "Image feature analysis and computer-aided diagnosis in mammography: Reduction of false-positive clustered microcalcifications using local edge-gradient analysis," Med. Phys. **22**, 161–169 (1995).
[126]X.-W. Xu and K. Doi, "Image feature analysis for computer-aided diagnosis: Detection of right and left hemidiaphragm edges and delineation of lung field in chest radiographs," Med. Phys. **23**, 1613–1624 (1996).
[127]M. L. Giger, J. M. Boone, and H.-P. Chan, "History and status of CAD and quantitative image analysis," Med. Phys. (in press).
[128]E. Chaney, G. Ibbott, and W. R. Hendee, "Methods for image segmentation should be standardized and calibrated," Med. Phys. **32**, 3507–3510 (2005).
[129]J. Duryea, M. Magalnick, S. Alli, L. Yao, M. Wilson, and R. Goldbach-Mansky, "Semiautomated three-dimensional segmentation software to quantify carpal bone volume changes on wrist CT scans for arthritis assessment," Med. Phys. **35**, 2321–2330 (2008).
[130]M. Hardisty, L. Gordon, P. Agarwal, T. Skrinskas, and C. Whyne, "Quantitative characterization of metastatic disease in the spine. Part I. Semiautomated segmentation using atlas-based deformable registration and the level set method," Med. Phys. **34**, 3127–3134 (2007).
[131]F. Zhuge, G. D. Rubin, S. Sun, and S. Napel, "An abdominal aortic aneurysm segmentation method: Level set with region and statistical information," Med. Phys. **33**, 1440–1453 (2006).
[132]E. Angelié, P. J. H. de Koning, M. G. Danilouchkine, H. C. van Assen, G. Koning, R. J. van der Geest, and J. H. C. Reiber, "Optimizing the automatic segmentation of the left ventricle in magnetic resonance images," Med. Phys. **32**, 369–375 (2005).
[133]F. Mao, J. Gill, D. Downey, and A. Fenster, "Segmentation of carotid

artery in ultrasound images: Method development and evaluation technique," Med. Phys. **27**, 1961–1970 (2000).
[134]J. D. Gill, H. M. Ladak, D. A. Steinman, and A. Fenster, "Accuracy and variability assessment of a semiautomatic technique for segmentation of the carotid arteries from three-dimensional ultrasound images," Med. Phys. **27**, 1333–1342 (2000).
[135]Y. Yuan, M. L. Giger, H. Li, K. Suzuki, and C. Sennett, "A dual-stage method for lesion segmentation on digital mammograms," Med. Phys. **34**, 4180–4193 (2007).
[136]K. Horsch, M. L. Giger, L. A. Venta, and C. J. Vyborny, "Automatic segmentation of breast lesions on ultrasound," Med. Phys. **28**, 1652–1659 (2001).
[137]W. Mullally, M. Betke, J. Wang, and J. P. Ko, "Segmentation of nodules on chest computed tomography for growth assessment," Med. Phys. **31**, 839–848 (2004).
[138]T. W. Way, L. M. Hadjiiski, B. Sahiner, H.-P. Chan, P. N. Cascade, E. A. Kazerooni, N. Bogot, and C. Zhou, "Computer-aided diagnosis of pulmonary nodules on CT scans: Segmentation and classification using 3D active contours," Med. Phys. **33**, 2323–2337 (2006).
[139]J. Wang, R. Engelmann, and Q. Li, "Segmentation of pulmonary nodules in three-dimensional CT images by use of a spiral-scanning technique," Med. Phys. **34**, 4678–4689 (2007).
[140]L. Drever, D. M. Robinson, A. McEwan, and W. Roa, "A local contrast based approach to threshold segmentation for PET target volume delineation," Med. Phys. **33**, 1583–1594 (2006).
[141]L. Drever, W. Roa, A. McEwan, and D. Robinson, "Iterative threshold segmentation for PET target volume delineation," Med. Phys. **34**, 1253–1265 (2007).
[142]D. W. G. Montgomery, A. Amira, and H. Zaidi, "Fully automated segmentation of oncological PET volumes using a combined multiscale and statistical model," Med. Phys. **34**, 722–736 (2007).
[143]M. Brambilla, R. Matheoud, C. Secco, G. Loi, M. Krengli, and E. Inglese, "Threshold segmentation for PET target volume delineation in radiation treatment planning: The role of target-to-background ratio and target size," Med. Phys. **35**, 1207–1213 (2008).
[144]T. Cootes, C. Taylor, D. Cooper, and J. Graham, "Active shape models—their training and application," Comput. Vis. Image Underst. **61**, 38–59 (1995).
[145]T. F. Cootes, G. J. Edwards, and C. J. Taylor, "Active appearance models," IEEE Trans. Pattern Anal. Mach. Intell. **23**, 681–685 (2001).
[146]S. M. Pizer, P. T. Fletcher, S. Joshi, A. G. Gash, J. Stough, A. Thall, G. Tracton, and E. L. Chaney, "A method and software for segmentation of anatomic object ensembles by deformable *m*-reps," Med. Phys. **32**, 1335–1345 (2005).
[147]J. Duryea and J. M. Boone, "A fully automated algorithm for the segmentation of lung fields on digital chest radiographic images," Med. Phys. **22**, 183–191 (1995).
[148]S. G. Armato III, M. L. Giger, K. Ashizawa, and H. MacMahon, "Automated lung segmentation in digital lateral chest radiographs," Med. Phys. **25**, 1507–1520 (1998).
[149]F. M. Carrascal, J. M. Carreira, M. Souto, P. G. Tahoces, L. Gómez, and J. J. Vidal, "Automatic calculation of total lung capacity from automatically traced lung boundaries in postero-anterior and lateral digital chest radiographs," Med. Phys. **25**, 1118–1131 (1998).
[150]B. van Ginneken and B. M. ter Haar Romeny, "Automatic segmentation of lung fields in chest radiographs," Med. Phys. **27**, 2445–2455 (2000).
[151]M. F. McNitt-Gray, H. K. Huang, and J. W. Sayre, "Feature selection in the pattern classification problem of digital chest radiograph segmentation," IEEE Trans. Med. Imaging **14**, 537–547 (1995).
[152]O. Tsujii, M. T. Freedman, and S. K. Mun, "Automated segmentation of anatomic regions in chest radiographs using an adaptive-sized hybrid neural network," Med. Phys. **25**, 998–1007 (1998).
[153]N. F. Vittitoe, R. Vargas-Voracek, and C. E. Floyd, Jr., "Markov random field modeling in posteroanterior chest radiograph segmentation," Med. Phys. **26**, 1670–1677 (1999).
[154]B. van Ginneken, M. Stegmann, and M. Loog, "Segmentation of anatomical structures in chest radiographs using supervised methods: A comparative study on a public database," Med. Image Anal. **10**, 19–40 (2006).
[155]D. Seghers, D. Loeckx, F. Maes, D. Vandermeulen, and P. Suetens, "Minimal shape and intensity cost path segmentation," IEEE Trans. Med. Imaging **26**, 1115–1129 (2007).
[156]Y. Shi, F. Qi, Z. Xue, L. Chen, K. Ito, H. Matsuo, and D. Shen, "Segmenting lung fields in serial chest radiographs using both population-based and patient-specific shape statistics," IEEE Trans. Med. Imaging **27**, 481–494 (2008).
[157]R. Pilgram, C. Walch, V. Kuhn, R. Schubert, and R. Staudinger, "Proximal femur segmentation in conventional pelvic x-ray," Med. Phys. **35**, 2463–2472 (2008).
[158]G. Bekes, E. Máté, L. G. Nyúl, A. Kuba, and M. Fidrich, "Geometrical model-based segmentation of the organs of sight on CT images," Med. Phys. **35**, 735–743 (2008).
[159]F. Zhuge, S. Sun, G. Rubin, and S. Napel, "A directional distance aided method for medical image segmentation," Med. Phys. **34**, 4962–4976 (2007).
[160]D. Ragan, G. Starkschall, T. McNutt, M. Kaus, T. Guerrero, and C. W. Stevens, "Semiautomated four-dimensional computed tomography segmentation using deformable models," Med. Phys. **32**, 2254–2261 (2005).
[161]R. Shekhar, P. Lei, C. R. Castro-Pareja, W. L. Plishker, and W. D. D'Souza, "Automatic segmentation of phase-correlated CT scans through nonrigid image registration using geometrically regularized free-form deformation," Med. Phys. **34**, 3054–3066 (2007).
[162]K. Wijesooriya, E. Weiss, V. Dill, L. Dong, R. Mohan, S. Joshi, and P. J. Keall, "Quantifying the accuracy of automated structure segmentation in 4D CT images using a deformable image registration algorithm," Med. Phys. **35**, 1251–1260 (2008).
[163]Z. Wu, E. Rietzel, V. Boldea, D. Sarrut, and G. C. Sharp, "Evaluation of deformable registration of patient lung 4DCT with subanatomical region segmentations," Med. Phys. **35**, 775–781 (2008).
[164]H. MacMahon, "Improvement in detection of pulmonary nodules: Digital image processing and computer-aided diagnosis," RadioGraphics **20**, 1169–1177 (2000).